Environmental Science: Atmospheres

ROYAL SOCIETY OF CHEMISTRY

PAPER

View Article Online
View Journal | View Issue

Cite this: *Environ. Sci.: Atmos.*, 2025, **5**, 67

Low temperature growth of sub 10 nm particles by ammonium nitrate condensation

Neil M. Donahue, *[a] Mao Xiao,[b] Ruby Marten,[b] Mingyi Wang,[ad] Weimeng Kong,[h] Meredith Schervish,[ac] Qing Ye,[a] Victoria Hofbauer,[a] Lubna Dada,[b] Jonathan Duplissy,[g] Henning Finkenzeller,[g] Hamish Gordon,[a] Jasper Kirkby,[fj] Houssni Lamkaddam,[b] Vladimir Makhmutov,[k] Maxim Philippov,[k] Birte Rörup,[g] Rainer Volkamer,[i] Dongyu Wang,[b] Stefan K. Weber,[j] Richard C. Flagan,[h] Dominik Stolzenburg[e] and Imad El Hadad[b]

Co-condensation of nitric acid and ammonia vapors to form ammonium nitrate transforms from a fully semi-volatile behavior when it is relatively warm (273 K and above, typical of the seasonal planetary boundary layer) into effectively non-volatile and irreversible uptake for the limiting vapor when it is cold (well below 273 K, typical of the upper troposphere and occasionally the wintertime boundary layer). This causes the system to switch in character from the one governed by semi-volatile equilibrium (how it is usually portrayed) to the one governed by irreversible reactive uptake to even the smallest particles. Uptake involves an activation diameter, which can be as small as 1 nm for typical vapor concentrations, and subsequent growth rates can be very high, exceeding 1000 nm h^{-1}. In addition to this somewhat surprising behavior, the system provides an exemplary case for semi-volatile reactive uptake within the context of volatility and saturation ratios.

Received 17th August 2024
Accepted 19th October 2024

DOI: 10.1039/d4ea00117f

rsc.li/esatmospheres

Environmental significance

Ammonium nitrate is a major constituent of submicron aerosol particles, and with rapidly decreasing sulfur emissions, it is likely to become even more important to submicron aerosol composition in the future. Though it is often treated with equilibrium thermodynamics in chemical transport models, when it is very cold, the condensation of the less abundant (rate limiting) vapor, either ammonia or nitric acid, becomes irreversible. This can drive growth of extremely small particles and may be a prominent growth mechanism in the parts of the upper troposphere such as the Asian tropopause aerosol layer, where nitrate is known to be a major aerosol constituent.

1 Introduction

In atmospheric aerosols, ammonium nitrate ($NH_4 \cdot NO_3$) is in many ways a quintessential example of semi-volatile reactive uptake, with strong temperature and humidity dependent partitioning between the gas-phase acid–base pair and the condensed-phase (aerosol) crystalline or dissolved salt.[1]

$$NH_3(v) + HONO_2(v) \overset{H_2O}{\rightleftarrows} NH_4 \cdot NO_3(a)$$

The equilibrium and volatility are affected by both water activity (for an aqueous solution) and of course temperature (for any aerosol phase). Both ammonia and nitric acid are by themselves highly volatile; nitric acid has a saturation vapor pressure of 117 Pa at a triple point of 235 K,[2] while ammonia has a saturation vapor pressure of 6063 Pa at a triple point of 195 K.[3] Consequently, by themselves, neither would be found in the condensed phase under any realistic conditions of Earth's atmosphere. It is only the proton transfer reaction to make the ionized salt solution that renders them at least semi volatile. The system thus serves as a canonical example of a condensed-phase reaction (proton transfer) that drives volatility.

[a]*Carnegie Mellon University, Department of Chemistry, Pittsburgh, PA, USA. E-mail: nmd@andrew.cmu.edu; Tel: +1 412 268-4415*
[b]*Laboratory for Atmospheric Chemistry, Paul Scherrer Institute, Villigen, Switzerland*
[c]*University of California, Irvine Department of Chemistry, Irvine, CA, USA*
[d]*University of Chicago Department of the Geophysical Sciences, Chicago, IL, USA*
[e]*Technical University of Vienna, Vienna, Austria*
[f]*Institute, for Atmospheric and Environmental Sciences, Goethe University Frankfurt, Altenhöferallee 1, 60438 Frankfurt am Main, Germany*
[g]*Institute for Atmospheric and Earth System Research/Physics, Faculty of Science, University of Helsinki, 00014 Helsinki, Finland*
[h]*Division of Chemistry and Chemical Engineering, California Institute of Technology, Pasadena, CA 91125, USA*
[i]*Department of Chemistry, University of Colorado, Boulder, CO 80305, USA*
[j]*CERN, Geneva, CH-1211, Switzerland*
[k]*P.N. Lebedev Physical Institute of the Russian Academy of Sciences, 119991 Moscow, Russia*

Because the individual constituents are so volatile and the equilibrium partitioning between the vapor and aerosol phases is so sensitive to temperature, most treatments of nitrate partitioning assume that (submicron) particles equilibrate rapidly,[4] though supermicron particles (often with different cations) require a dynamical treatment.[5] Because of this, ammonium nitrate has rarely been regarded as important to nucleation and growth of nanoparticles. However, when it is cold enough and when there is a sufficient quantity (production or emission rate) of ammonia and nitric acid, ammonium nitrate will participate in the growth of extremely small particles and eventually nucleation itself.[6–9] Our objective here is to explore the transition of ammonium nitrate partitioning from an essentially semi-volatile nature to an effectively non-volatile (irreversible in the limiting vapor) behavior.

2 Setup

We are interested in the transition of ammonium nitrate partitioning from being qualitatively "semi volatile" at relatively high temperature to qualitatively "irreversible" at lower temperature. In this case the individual constituents remain volatile under all relevant atmospheric conditions, but the equilibrium reaction to an effectively non-volatile salt becomes effectively irreversible and ultimately rate-limited by uptake of the limiting vapor. Because we are interested in the low temperature behavior, here we shall consider only the solid, crystalline phase of ammonium nitrate. We need to consider three fully reversible processes:

$$NH_3(v) \rightleftarrows NH_3(s) \quad (R1)$$

$$HONO_2(v) \rightleftarrows HONO_2(s) \quad (R2)$$

$$NH_3(s) + HONO_2(s) \rightleftarrows NH_4{\cdot}NO_3(s) \quad (R3)$$

A full treatment, especially with other ions and for aqueous solutions, would break reaction R3 into its elementary steps as well.

$$HONO_2(s) \rightleftarrows NO_3^- + H^+$$

$$NH_3(s) + H^+ \rightleftarrows NH_4^+$$

$$NH_4^+ + NO_3^- \rightleftarrows NH_4{\cdot}NO_3(s)$$

However, as we are considering pure, solid ammonium nitrate we omit these reactions here.

The experimental evidence motivating this analysis is observations from the CERN CLOUD experiment demonstrating that systems containing mixtures of sulfuric acid, nitric acid, and ammonia (and in some cases oxidized organics) show clear evidence for nucleation followed by activation and very rapid growth (20–2000 nm h^{-1}) of small particles with 1.7 nm < d_p < 15 nm. The experiments were designed to mimic conditions of a wintertime megacity and were thus carried out at 263 K and 278 K, with 1 ppbv < χ_{NH_3} < 3 ppbv and 10 pptv < χ_{HONO_2} < 1000 pptv. The observed activation diameters and growth rates are shown in Fig. 1.[6] Both the activation diameters and the growth rates showed an empirical relationship to the product $\chi_{HONO_2}{\cdot}\chi_{NH_3}$. This is expected for activation as it is fundamentally related to the saturation ratio of the vapors, and for this second-order process the saturation ratio involves the product of the vapor concentrations (activities). However, the quadratic growth-rate dependence is more of a surprise, as one might expect the growth rate to depend only on the concentration of the limiting vapor to an expected stoichiometric uptake.

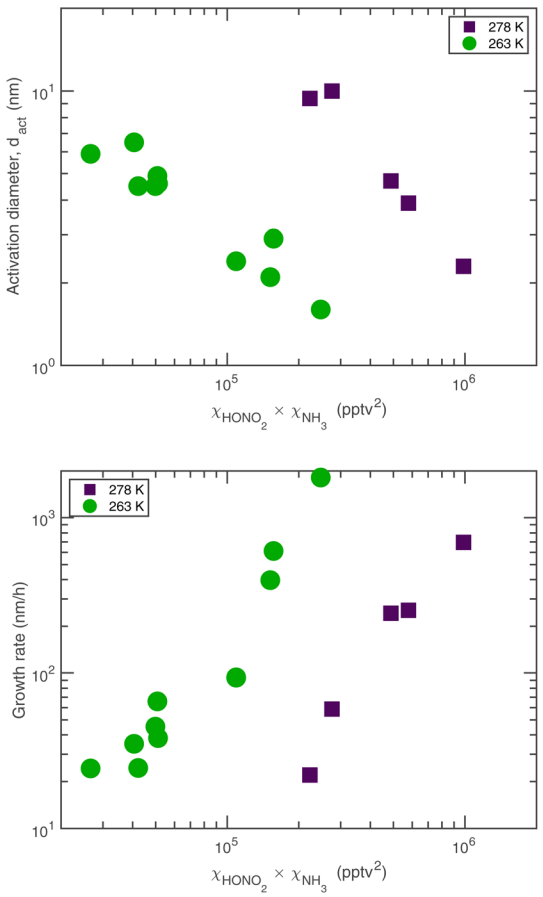

Fig. 1 Activation diameter (top) and activated growth rate (bottom) of particles *via* ammonium nitrate condensation observed in the CERN CLOUD experiment. Both are proportional to the product of nitric acid and ammonia vapors, and both shift by roughly a factor of 10 at 263 K (green circles) *vs.* 278 K (purple squares). Growth rates can exceed 1000 nm h^{-1} with activation diameters as small as 1.5 nm.

3 Thermodynamics

For our calculations we need to know the saturation vapor pressure of ammonia, $p^\circ_{NH_3}$, the saturation vapor pressure, p°_i, of nitric acid, $p^\circ_{HONO_2}$, and the equilibrium constant for ammonium nitrate formation in a condensed phase containing pure saturated ammonium nitrate, K^{eq}_{R3}. From this we can determine activities, a, and the reactive activity product in the vapor (v) and suspended (s) phases. The gas-phase activity at pressure, p, and temperature, T, is the saturation ratio with

respect to partial pressure (p_i), vapor concentration (c_i^{v}), or vapor mole fraction (mixing ratio, x_i^{v}):

$$a_i^{\mathrm{v}} = \frac{p_i}{p_i^\circ} = \frac{c_i^{\mathrm{v}} k_{\mathrm{B}} T}{p_i^\circ} = \frac{x_i^{\mathrm{v}} p}{p_i^\circ}$$
$$a_{\mathrm{NH_3}}^{\mathrm{s}} a_{\mathrm{HONO_2}}^{\mathrm{s}} = \frac{1}{K_{\mathrm{R3}}^{\mathrm{eq}}} \quad (1)$$

The condensed-phase (suspended) activity is the product of a fraction (mole, $x_{i,p}$; mass, $w_{i,p}$, and volume) and the appropriate activity coefficient (mole, $\eta_{i,p}$; mass, $\zeta_{i,p}$):

$$a_{i,p}^{\mathrm{s}} = \eta_{i,p} x_{i,p}^{\mathrm{s}} = \zeta_{i,p} w_{i,p}^{\mathrm{s}} \quad (2)$$

In practice, values are known for the overall equilibrium between the condensed phase and the vapor, giving the vapor activity product,[1] but it is informative to separate out the gas-particle partitioning of the unreacted vapors and the particle-phase proton-transfer reaction as we have done in order to illustrate the overall process. All of the processes are "functionally" reversible, making this a true semi-volatile system. We need to know the physical and thermodynamic properties of all constituents to describe the dynamics. Ultimately the accuracy for this system depends on the overall (vapor to salt) equilibrium and so we ensure that the individual vapor pressures and condensed-phase equilibrium constant are consistent with the more accurate overall equilibrium constant.[1]

3.1 Ammonia

Ammonia is extremely volatile. The molar mass is

$$M_{\mathrm{NH_3}} = 17.03026 \times 10^{-3}\ \mathrm{kg\ mol^{-1}}$$

Its triple point properties are

$$T_{t,\mathrm{NH_3}} = 195.48\ \mathrm{K}$$
$$p_{t,\mathrm{NH_3}} = 6063\ \mathrm{Pa}$$
$$\rho_{t,\mathrm{NH_3}}^{l} = 733.74\ \mathrm{kg\ m^{-3}}$$

3.1.1 NH_3 functions. The density and saturation vapor pressure of ammonia were reported by Haar and Gallagher at NIST (NBS) in the 1970s.[3]

$$\rho_{\mathrm{NH_3}}^{l} = [636 - 1.43(T/^\circ\mathrm{C})]\mathrm{kg\ m^{-3}}$$
$$\ln\left(p_{\mathrm{NH_3}}^\circ / \mathrm{atm}\right) = A/T + B + CT + DT^2 + ET^3$$
$$A = -3684.7798\ \mathrm{K}$$
$$B = 20.428787$$
$$C = -0.02893289$$
$$D = 3.4798128 \times 10^{-5}$$
$$E = -9.2219845 \times 10^{-9}$$

or since 1 atm = 1.01325×10^5 Pa, B/Pa = 31.9549. This all gives the vapor pressure plot under atmospheric conditions shown in Fig. 2. That is such an enormous value it is worth considering the gas-phase activity of a reference level of ammonia. For this we shall consider a mole fraction of 1 ppbv, meaning a partial pressure of $p_{\mathrm{NH_3}} = 10^{-4}$ Pa. Fig. 3 shows the gas-phase activity ($a_{\mathrm{NH_3}}^{\mathrm{v}} = p_{\mathrm{NH_3}}^\circ / p_{\mathrm{NH_3}}$) of 1 ppbv of ammonia. Even at 200 K it is 10^{-8} and at 280 K it is just above 10^{-10}. The gas-phase activity of 1 ppbv of ammonia at +5 °C is 2.0×10^{-10} while at −10 °C it is 3.5×10^{-10}.

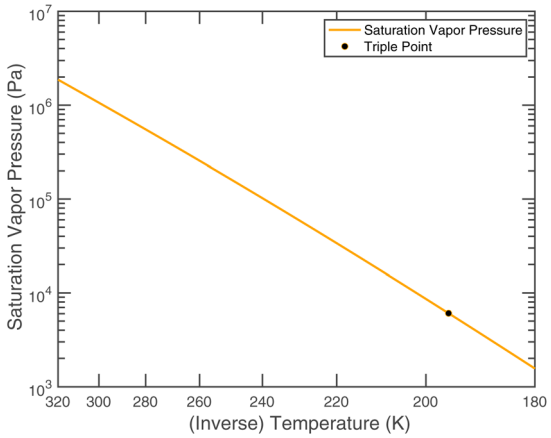

Fig. 2 Saturation vapor pressure of ammonia over a pure liquid.

3.2 Nitric acid

Nitric acid is also quite volatile, with a molar mass

$$M_{\mathrm{HONO_2}} = 63.012 \times 10^{-3}\ \mathrm{kg\ mol^{-1}}$$

Combining values from Mozurkewich[1] and the saturation vapor pressure from Duisman.[2]

$$T_{t,\mathrm{HONO_2}} = 235\ \mathrm{K}$$
$$p_{t,\mathrm{HONO_2}} = 117\ \mathrm{Pa}$$
$$\rho_{t,\mathrm{HONO_2}}^{l} = 1513\ \mathrm{kg\ m^{-3}}$$

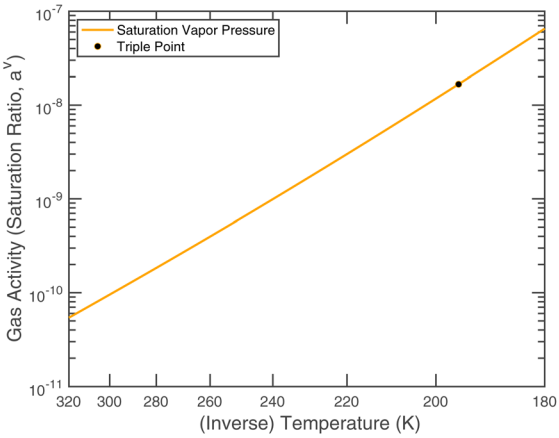

Fig. 3 Saturation ratio (gas-phase activity) of 1 ppbv of ammonia over a pure liquid.

3.2.1 $HONO_2$ functions. The density and saturation vapor pressure of nitric acid were reported by Duisman at Union Carbide.[2]

$$\rho^{l}_{HONO_2} = 1510 \text{ kg m}^{-3}$$
$$\ln\left(p^{\circ}_{HONO_2}/\text{torr}\right) = A/(T + 230\ ^{\circ}\text{C}) + B$$
$$A = -1486.238\ ^{\circ}\text{C}$$
$$B = 7.61628$$
$$\ln\left(p^{\circ}_{HONO_2}/\text{torr}\right) = A/(T + 230 - 273.15) + B$$
$$= A/(T - 43.15\text{ K}) + B$$
$$\ln\left(p^{\circ}_{HONO_2}/\text{Pa}\right) = A/(T - 43.15\text{ K}) + B + 4.8928$$
$$B' = 12.5091$$

Nitric acid has a lower vapor pressure than ammonia but not by all that much, as we see in Fig. 4. Thus, again for a reference mixing ratio of 1 ppbv, the gas-phase activities in Fig. 5 are about 2×10^{-7} at 280 K and 4×10^{-6} at 200 K (over a supercooled liquid solution, not nitric acid trihydrate or anything like that). The gas-phase activity of 1 ppbv of ammonia at +5 °C is 2.1×10^{-7} while at −10 °C it is 3.2×10^{-7}.

3.3 Ammonium nitrate

Finally, ammonium nitrate has the following properties:

$$M_{NH_4\cdot NO_3} = 80.044 \times 10^{-3} \text{ kg mol}^{-1}$$
$$\rho_{NH_4\cdot NO_3} = 1725 \text{ kg m}^{-3}$$

Given the density of ammonium nitrate we can easily calculate the number of $NH_4\cdot NO_3$ per particle *vs.* diameter, as shown in Fig. 6.

3.3.1 Equilibrium. Thermodynamic data are known for ammonium nitrate equilibrium directly between the vapor and condensed phase[1]

$$NH_3(v) + HONO_2(v) \rightleftarrows NH_4\cdot NO_3(s)$$

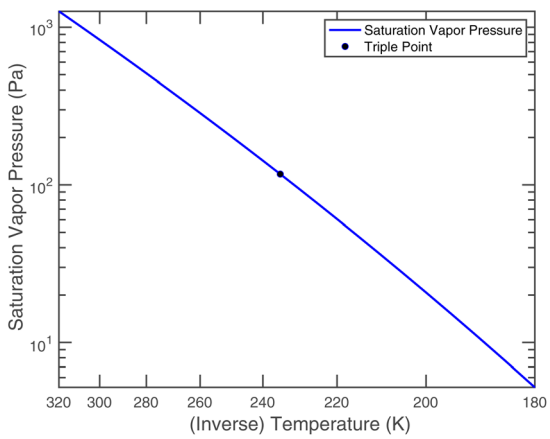

Fig. 4 Saturation vapor pressure of nitric acid over a pure liquid.

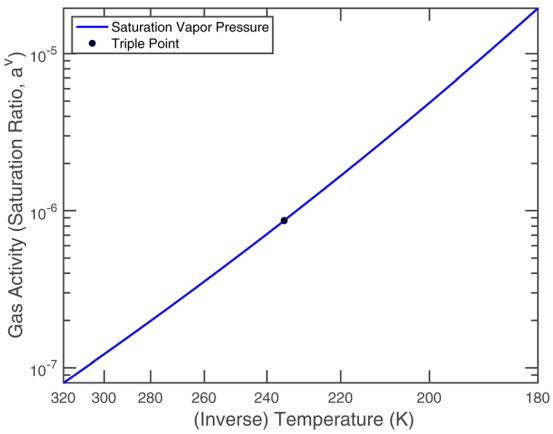

Fig. 5 Saturation ratio (gas-phase activity) of 1 ppbv of nitric acid over a pure liquid.

However, we can consider the equilibrium of reaction R3, where in terms of activity the equilibrium can be written as

$$K^{eq}_{R3} = \frac{a^{s}_{NH_4\cdot NO_3}}{a^{s}_{NH_3}\cdot a^{s}_{HONO_2}} \simeq \frac{1}{a^{s}_{NH_3}\cdot a^{s}_{HONO_2}}.$$

Here, we make use of the negligibly small activities of the undissociated molecules in the suspended particle phase at equilibrium with the vapor partial pressures we have already calculated. For our purposes, over a flat surface the gas-particle system is at equilibrium for 100 pptv of ammonia and about 2 ppbv of nitric acid at +5 °C and about 20 pptv of nitric acid at −10 °C.

The overall equilibrium between vapor and a saturated condensed phase of ammonium nitrate can be expressed *via* a dissociation constant for

$$NH_4\cdot NO_3 \rightleftarrows NH_3(v) + HONO_2(v)$$

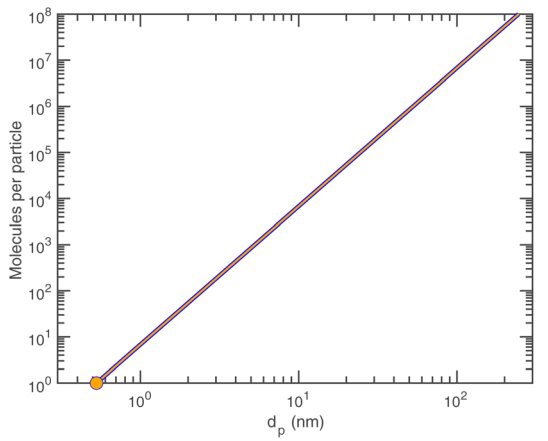

Fig. 6 Molecules per particle of pure ammonium nitrate.

$$K_p = p_{NH_3} p_{NHO_3} = \left(a^v_{NH_3} \cdot a^v_{HONO_2}\right)\left(p^\circ_{NH_3} \cdot p^\circ_{NHO_3}\right)$$

$$K_p = \frac{p^\circ_{NH_3} p^\circ_{NHO_3}}{K^{eq}_{R3}}$$

$$\ln(K^{eq}_{R3}) = -\ln(K_p) + \ln\left(p^\circ_{NH_3}\right) + \ln\left(p^\circ_{NHO_3}\right)$$

Mozurkewich[1] gives an overall dissociation constant for solid-vapor (in $nb^2 = 10^{-8}$ Pa^2) of

$$\ln\left(K_p/nb^2\right) = 118.87 - \frac{24\,084}{T} - 6.025\ln(T)$$

$$\ln\left(K_p/Pa^2\right) = 100.45 - \frac{24\,084}{T} - 6.025\ln(T)$$

An effective Arrhenius activation energy for the equilibrium coefficient is 18 150 K; it is extremely temperature dependent. It is important to emphasize again that this overall equilibrium is well constrained, and the individual condensed-phase equilibrium coefficient and the vapor pressures only provide useful insights. Fig. 7 shows that most of the temperature dependence comes from the ammonium nitrate dissociation, which spans 18 orders of magnitude over the atmospheric temperature range (compared with 2 or 3 decades for the vapor pressures). This is why the potential for relatively rapid growth (rather than equilibrium ammonium nitrate formation in larger particles) is confined to low temperature regions of the atmosphere.

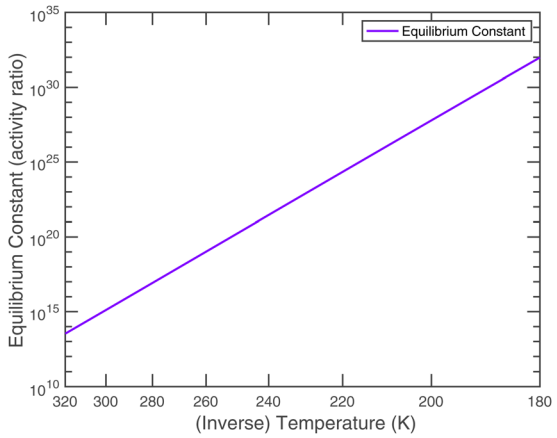

Fig. 7 Equilibrium constant for ammonium nitrate formation in the condensed phase.

4 Microphysics

With the thermodynamics (vapor pressures and equilibrium coefficients) known, we can now consider the microphysics of collisions. We will use a microphysical formulation grounded in the kinetic regime of molecular (and particle) collisions, rather than the bulk fluid continuum regime of diffusion to and from particles. This is because we are most interested in condensation to particles with $2 \lesssim d_p \lesssim 100$ nm, where the Knudsen number $Kn \gtrsim 1$ and microphysics are more kinetic than not.

The net condensation flux of a species with vapor concentration c^v_i and saturation concentration $c^\circ_i = p^\circ_i/(k_B T)$ to a suspension of identical particles p with number concentration N^s_p and (physical) diameter d_p depends fundamentally on the collision cross section, $\sigma_{i,p}$, the collision speed, $s'_{i,p}$, and the thermodynamic excess concentration, $c^{xs}_{i,p}$.[10] This can also be expressed in terms of the (effective spherical) particle surface area, A^s_p and the (effective perpendicular) collision speed of molecules with that surface, $s^\perp_{i,p}$, but with several modifying factors that we define below.

$$\phi^{v,s}_{i,p} = \underbrace{N^s_p\left(\frac{\pi}{4}(d_p + d_i)^2 \alpha_{i,p} E^\mu_{i,p}\right)}_{\text{cross section: } \sigma_{i,p}} \underbrace{\overline{s}_{i,p} B_{i,p}}_{\text{speed: } s'_{i,p}} \underbrace{\left[c^v_i - a^s_{i,p} K_{i,p} c^\circ_i\right]}_{\text{excess conc.: } c^{xs}_{i,p}} = \underbrace{N^s_p \pi d_p^{\,2}}_{\text{area: } A^s_p} \underbrace{\left(E^\mu_{i,p} \varepsilon_{i,p} e_{i,p} \alpha_{i,p} \frac{\overline{s}_i}{4} B_{i,p}\right)}_{\text{collision speed: } s^\perp_{i,p}} \underbrace{\left[c^v_i - a^s_{i,p} K_{i,p} c^\circ_i\right]}_{\text{excess conc.: } c^{xs}_{i,p}}$$

$$\text{flux per unit surface area: } \phi^{v,s}_{i,p}$$

Note that the diameter is the physical diameter, not the mobility diameter (which is typically $d_{mob} \simeq d_p + 0.3$ nm).[11]

The flux of the condensing species per unit particle surface area is

$$\begin{aligned}\phi^{v,s}_{i,p} &= s^\perp_{i,p} c^{xs}_{i,p} = s^\perp_{i,p} c^\circ_i \left[a^v_i - a^s_{i,p} K_{i,p}\right] \\ &= s^\perp_{i,p} c^\circ_i a^v_i \left[1 - \frac{a^s_{i,p}}{a^v_i} K_{i,p}\right] \\ &= s^\perp_{i,p} \gamma_{i,p} c^v_i;\ \gamma_{i,p} = \left[1 - \frac{a^s_{i,p}}{a^v_i} K_{i,p}\right]\end{aligned} \tag{3}$$

This depends on the collision speed, the vapor concentration, and an uptake coefficient, $\gamma_{i,p}$, that in turn depends on the activities in both phases as well as a Kelvin term, $K_{i,p}$ for curvature effects over very small particles. The flux is either number per unit area or mass per unit area depending on the concentration units.

The collision speed, $s^\perp_{i,p}$, is the effective line-of-centers velocity of each vapor toward the particle surface, accounting for enhancements (*i.e.* van der Waals, vapor size, reduced mass) and limitations (*i.e.* accommodation, gas-phase diffusion near the particle). It is derived from the average molecular speed, $\overline{s}_i = \sqrt{8 k_B T/(\pi m_i)}$. van der Waals interactions between the vapor and particle (charge-dipole, dipole-induced dipole, and induced dipole-induced dipole) can be represented as an

enhancement over hard-sphere collisions, $E^{\mu}_{i,p} = E^{\mu}(A_{i,p})$, where $A_{i,p}$ is the Hamaker constant in joule.[12,13] The non-zero size of the vapor is accounted for by $\varepsilon_{i,p} = (d_i^2 + d_p^2)/d_p^2$, and the non-infinite mass of small clusters gives a reduced-mass correction of $e_{i,p} = \sqrt{(m_i + m_p)/m_p}$.[10] The mass accommodation coefficient, $\alpha_{i,p}$ is likely 1.[14] Gas-phase diffusion limitations emerging for small Knudsen numbers are given by $B_{i,p}$.[10,15]

The excess concentration, sometimes also known as the thermodynamic driving force, can be written as

$$c^{\mathrm{xs}}_{i,p} = F^{\mathrm{v,s}}_{i,p} = c^{\circ}_i \left[a^{\mathrm{v}}_i - a^{\mathrm{s}}_{i,p} K_{i,p} \right] \tag{4}$$

The Kelvin term $K_{i,p}$ scales with a "Kelvin diameter" for decadal change, d_{K10}. We use base-10 because it is a little easier to think in decades; for particles with $d_p = d_{\mathrm{K10}}$, condensed-phase activity is increased by a factor of 10.

$$\begin{aligned} \log_{10} K_{i,p} &= \left(\frac{d_{\mathrm{K10}}}{d_p} \right) + \mathrm{O}\left(\frac{d_{\mathrm{K10}}}{d_p} \right)^2 + \ldots \\ d_{\mathrm{K10}} &= 0.434\, d_{\mathrm{K}}; d_{\mathrm{K}} = \left(\frac{4\sigma_p m_i}{k_B T \rho_i} \right) \end{aligned} \tag{5}$$

This relates the bulk properties (σ_i, ρ_p) to the molecular properties of clusters *via* the correspondence principle (potentially with higher-order terms). It is perhaps not widely recognized how small d_{K10} actually is; it is the diameter where the effective saturation concentration increases by 1 decade, and for typical surface tensions and densities, $d_{\mathrm{K10}} \simeq$ 4–5 nm. Still, for $d_p = 1$ nm, $K_{i,p} = 10^4$–10^5, which is why, in classical nucleation theory, very high supersaturations can be required to surmount the critical cluster. This is crucial to the activation behavior observed in ammonium-nitrate condensation in Fig. 1.

We can express the excess concentration as the product of the vapor concentration and an uptake coefficient, $\gamma_{i,p}$ (the fraction of collisions resulting in uptake), defined in eqn (3). We can re-write this in terms of the saturation ratio (including curvature), $S_{i,p}$, and the excess saturation ratio, $S^{\mathrm{xs}}_{i,p} = S_{i,p} - 1$.

$$\begin{aligned} S_{i,p} &= \frac{a^{\mathrm{v}}_i}{a^{\mathrm{s}}_{i,p} K_{i,p}} \\ \gamma_{i,p} &= \left[1 - \frac{1}{S_{i,p}} \right] = \frac{S_{i,p} - 1}{S_{i,p}} = \frac{S^{\mathrm{xs}}_{i,p}}{S_{i,p}} \end{aligned} \tag{6}$$

The uptake coefficient is simply the fractional excess saturation ratio over a small, curved particle: the ratio of the "Kelvin adjusted" suspended-phase activity, $a^{\mathrm{s}}_i K_{i,p}$, to the equilibrium suspended-phase activity, which would be a^{v}_i. For example, for water vapor during cloud droplet activation, the fractional excess saturation ratio is typically 0.002–0.01, so between 1% and 0.2% of water vapor collisions are taken up (assuming a mass accommodation coefficient, $\alpha = 1$). If the system is at equilibrium, $\gamma_{i,p} = 0$, whereas for kinetic uptake on every collision with the surface, $\gamma_{i,p} = 1$. The uptake coefficient is thus just the fractional excess saturation ratio (at the surface – we neglect any condensed phase diffusion limitations, which in any event are irrelevant for this pure model system).

The growth rate, $R^{\mathrm{gr}}_{i,p}$, is proportional to the flux per unit surface area, $\phi^{\mathrm{v,s}}_{i,p}$. Assuming a spherical particle (or a spherical equivalent d_p), the growth rate due to condensation of a given species is

$$\begin{aligned} R^{\mathrm{gr}}_{i,p} &= \frac{\mathrm{d}d_p}{\mathrm{d}t_i} = 2 V_{i,p} \phi^{\mathrm{v,s}}_{i,p} \left([c_i] = \#\mathrm{volume}^{-3} \right) \\ &= \frac{2}{\rho_{i,p}} \phi^{\mathrm{v,s}}_{i,p} \left([c_i] = \mathrm{mass\ volume}^{-3} \right) \end{aligned} \tag{7}$$

The factor of 2 is because growth extends the diameter by extending the radius symmetrically about the sphere. The molecular volume in the particle is $V_{i,p} = m_{i,p}/\rho_{i,p}$; we retain the $\{i, p\}$ "species within particle" designation to account for the form of the species within the particle. Specifically in the case we are considering here, one mole of either ammonia or nitric acid condensation will result in one mole of ammonium nitrate, and so the appropriate mass and density are those of ammonium nitrate. More generally, we could write $\delta V_{i,p}$ as the change in particle volume arising from condensation of this species; here we can also treat condensation of water vapor for deliquesced and/or aqueous particles.

We can solve eqn (7) for any given parameter, but for the most part we will either want to know the growth rate for a given vapor concentration c^{v}_i or mixing ratio x^{v}_i or conversely find either of those in terms of a given growth rate:

$$R^{\mathrm{gr}}_{i,p} = 2 V_{i,p} s^{\perp}_{i,p} \gamma_{i,p} c^{\mathrm{v}}_i = 2 V_{i,p} s^{\perp}_{i,p} \gamma_{i,p} x^{\mathrm{v}}_i c^{\mathrm{c}}_{\mathrm{M}} \tag{8}$$

We also may want to identify the maximum possible growth rate, when $\gamma_{i,p} = 1$:

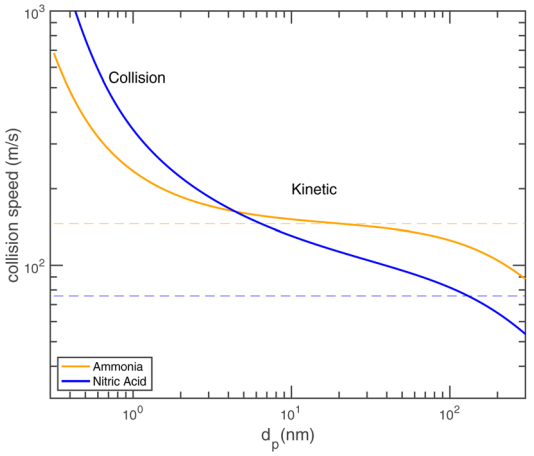

Fig. 8 Collision speed $s^{\perp}_{i,p}$ for NH_3 and $HONO_2$ *vs.* the particle diameter with $A_{HONO_2} = 6 \times 10^{-20}$ joule and $A_{NH_3} = 0$ joule. Dashed horizontal lines are asymptotic values equal to one-quarter of the average gas speed. This is the so-called "kinetic" limit of nominally constant growth; for $d_p \simeq 10$ nm the NH_3 speed exhibits a modest plateau near the "kinetic" value. For very small particles, the size of the molecule, (small) mass of the particle, and the interaction potential between them all enhance the speed in the free-molecular or "collision" limit.

$$R_{i,p}^{\max} = 2V_{i,p}s_{i,p}^{\perp}c_i^{\mathrm{v}} = 2V_{i,p}s_{i,p}^{\perp}x_i^{\mathrm{v}}c_{\mathrm{M}}^{\mathrm{v}} \quad (9)$$

The concentration of all (air) molecules is $c_{\mathrm{M}}^{\mathrm{v}}$.

Fig. 8 shows the collision speeds for both NH_3 and $HONO_2$, including the "kinetic regime" asymptote $s_i^{\perp,\mathrm{kin}} = \overline{s_i}/4$. This assumes Hamaker constants of $A_{\mathrm{HONO_2}} = 6 \times 10^{-20}$ joule and $A_{\mathrm{NH_3}} = 0$ joule, because $HONO_2$ has a larger dipole moment than NH_3. Values are based on growth rate observations for $H_2SO_4 \rightarrow (NH_4)_2{\cdot}SO_4$ (ref. 15) because the dipole moment of $HONO_2$ vapor is similar to the dipole moment of H_2SO_4 vapor and the relative values appropriate for $(NH_4){\cdot}NO_3$ *vs.* $(NH_4)_2{\cdot}SO_4$ are not known. The exact values are not overly important to this example, but the difference between a highly polar but relatively heavy acid and a non-polar but light base is interesting and illustrative. As Fig. 8 shows, NH_3 has a speed advantage above 5 nm, but for very small particles the van der Waals effect (as well as the molecular size and reduced mass effects) give $HONO_2$ a speed advantage. Growth by ammonium nitrate formation ultimately means a 1 : 1 uptake frequency for NH_3 and $HONO_2$, and this collision speed transition means that in some circumstances a system can go from being NH_3 limited for the smallest particles to $HONO_2$ limited for larger particles.

5 Semivolatile condensation

Let us consider a flux balance for ammonium nitrate uptake. For the sake of simplicity and generality of (mono)acid–base condensation we shall refer to $HONO_2$ as A and NH_3 as B.

5.1 Setup

Because of the 1 : 1 stoichiometry enforced by the reactive uptake, there will be a stoichiometric, molar, flux balance:

$$\begin{aligned}
&\phi_{\mathrm{A},p}^{\mathrm{v,s}} = \phi_{\mathrm{B},p}^{\mathrm{v,s}} \\
&s_{\mathrm{B},p}^{\perp}c_{\mathrm{B}}^{\mathrm{v}}\gamma_{\mathrm{B},p} = s_{\mathrm{A},p}^{\perp}c_{\mathrm{A}}^{\mathrm{v}}\gamma_{\mathrm{A},p} \\
&\gamma_{\mathrm{B},p} = \frac{s_{\mathrm{A},p}^{\perp}c_{\mathrm{A}}^{\mathrm{v}}}{s_{\mathrm{B},p}^{\perp}c_{\mathrm{B}}^{\mathrm{v}}}\gamma_{\mathrm{A},p} \\
&\gamma_{\mathrm{B},p} = r_{\mathrm{AB}}^{\mathrm{v}}\gamma_{\mathrm{A},p} \\
&r_{\mathrm{AB}}^{\mathrm{v}} = \frac{s_{\mathrm{A},p}^{\perp}c_{\mathrm{A}}^{\mathrm{v}}}{s_{\mathrm{B},p}^{\perp}c_{\mathrm{B}}^{\mathrm{v}}}
\end{aligned} \quad (10)$$

Here we define a collision ratio of A and B with the surface, $r_{\mathrm{AB}}^{\mathrm{v}}$. This is the concentration ratio of the two species scaled by the collision speed for each molecule seen in Fig. 8. Eqn (10) is symmetrical, but it is easier to think of the case where $r_{\mathrm{AB}}^{\mathrm{v}} \geq 1$ so that A is in excess and B is the rate-limiting contributor to condensational growth. In the limit of $r_{\mathrm{AB}}^{\mathrm{v}} \gg 1$, there is a large excess of A and we expect A to be equilibrated ($a_{\mathrm{A},p}^{\mathrm{s}}K_{\mathrm{A},p} \rightarrow a_{\mathrm{A}}^{\mathrm{v}}$), so $\gamma_{\mathrm{A},p} \rightarrow 0$.

When the collision ratio $r_{\mathrm{AB}}^{\mathrm{v}} = 1$, the system is at the "equi-collision" point where with stoichiometric uptake we must have $\gamma_{\mathrm{A}} = \gamma_{\mathrm{B}}$. For large excess saturation, $\gamma = 1$. In the real case we are considering, NH_3 (B) is about twice as fast as $HONO_2$ (A), so the equi-collision point occurs when $c_{\mathrm{HONO_2}} \simeq 2c_{\mathrm{NH_3}}$ (A : B $\simeq$ 2).

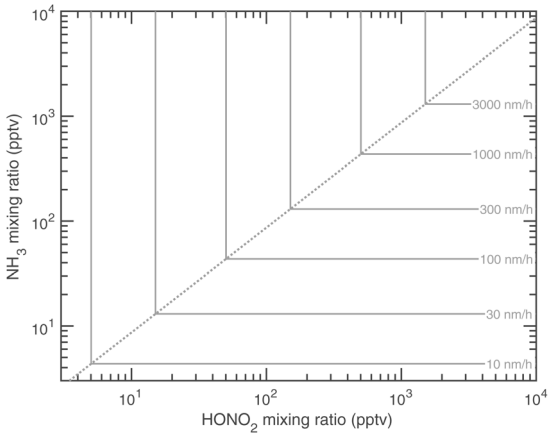

Fig. 9 Maximum growth rates of 10 nm particles at 263 K for ammonium nitrate formation. Growth rates are shown as contour labels. The maximum depends sharply on the limiting vapor, with ammonia limitation causing horizontal contours at relatively high nitric acid and nitric acid limitation causing vertical contours at relatively high ammonia. The spine is offset from 1 : 1 based on the relative vapor speeds and depends on particle size.

The maximal growth rates, for $\gamma = 1$, form a chevron meeting along this "equi-collision" line, as shown in Fig. 9 for d_{p} = 10 nm. This shows that a few 100 pptv of either NH_3 or $HONO_2$ have the potential to drive particle growth at $s^{\mathrm{gr}} > 100$ nm h^{-1}, provided that there is enough driving force (supersaturation) for this to actually occur. As a point of reference, growth rates between 1 and 10 nm h^{-1} are typical of the continental boundary layer when conditions permit accurate determination of aerosol growth.[16,17]

However, we also have the ammonium nitrate equilibrium to consider. Here we assume rapid equilibration of the salt with the undissociated molecules in the suspended particle phase (slow particle phase kinetics is a completely different limit, mostly controlled by volatility). This imposes a balance on the activity product in the particles.

$$a_{\mathrm{A}}^{\mathrm{s}}a_{\mathrm{B}}^{\mathrm{s}} = \frac{1}{K_{\mathrm{AB}}^{\mathrm{eq}}} \text{ or } a_{\mathrm{A}}^{\mathrm{s}} = \frac{1}{a_{\mathrm{B}}^{\mathrm{s}}K_{\mathrm{AB}}^{\mathrm{eq}}} \quad (11)$$

The overall saturation of vapors toward the particle phase can be written as

$$S_{\mathrm{AB},p} = \frac{a_{\mathrm{A}}^{\mathrm{v}}a_{\mathrm{B}}^{\mathrm{v}}}{a_{\mathrm{A}}^{\mathrm{s}}a_{\mathrm{B}}^{\mathrm{s}}K_{\mathrm{A},p}K_{\mathrm{B},p}} = \frac{a_{\mathrm{A}}^{\mathrm{v}}a_{\mathrm{B}}^{\mathrm{v}}K_{\mathrm{AB}}^{\mathrm{eq}}}{K_{\mathrm{A},p}K_{\mathrm{B},p}} = \frac{a_{\mathrm{A}}^{\mathrm{v}}a_{\mathrm{B}}^{\mathrm{v}}K_{\mathrm{AB}}^{\mathrm{eq}}}{K_{\mathrm{AB},p}^{2}} \quad (12)$$

This is the product of the vapor activities (saturation ratios) and suspended particle phase activities (including curvature) and it is the fundamental imposed thermodynamic driver for growth. The two Kelvin terms multiply, which we represent as the square based on the average of the two Kelvin diameters, $d_{\mathrm{K10,AB}} = 0.5 \times (d_{\mathrm{K10,A}} + d_{\mathrm{K10,B}})$.

The overall equilibrium between vapor concentrations and the salt is what is best constrained by thermodynamic data and calculations (without the Kelvin effect).[1] As Fig. 10 shows, for

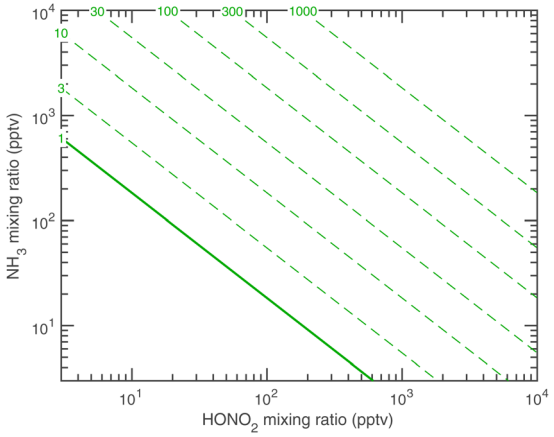

Fig. 10 Saturation ratio over a pure ammonium nitrate crystalline surface at 263 K *vs.* nitric acid and ammonia mixing ratios. The solid green diagonal shows $S = 1$. Regions to the lower left are undersaturated and particles will evaporate; those to the upper right, with saturation ratios indicated on the dashed contours, are super saturated and particles will grow. The saturation threshold moves toward the lower left as temperature falls and towards the upper right as it increases.

sub-freezing conditions (263 K) the saturation isopleths over a flat surface cut through typical ambient (urban) mixing ratios of NH_3 and $HONO_2$.

We have two constraints on the actual growth rate. One is the maximum possible growth rate shown in Fig. 9, and the other is the saturation ratio, $S_{AB,p}$, shown in Fig. 10, both at 263 K. These two combine to give the overall constraints to growth, as shown in Fig. 11. We expect the actual growth rate to be at the maximum value for $S_{AB,p} \gg 1$, but obviously much lower for $S_{AB,p} \gtrsim 1$, where the natural quantity is the excess saturation, $S_{AB,p} - 1$. Of course, for $S_{AB,p} < 1$ there is no growth, and the dynamics turn to evaporation.

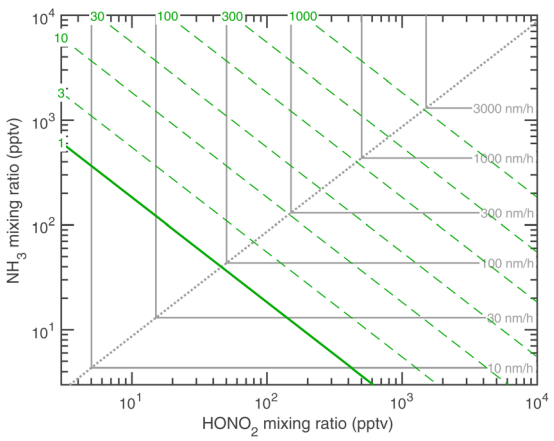

Fig. 11 Phase space combining maximum growth rates and the saturation ratio over an ammonium nitrate surface at 263 K. Only systems in the saturated region to the upper right of the solid green saturation contour ($S = 1$) will grow, and growth near $S = 1$ will be (much) slower than the maximum possible values.

The collision rates and thus the maximum growth rates are only a weak function of temperature, whereas the saturation ratios (at a fixed concentration or mixing ratio) are extremely strong functions of temperature. The saturation limits will thus sweep from the lower left of Fig. 11 toward the upper right as temperature increases.

5.2 Activation diameter

Before anything grows, the growth must start. This is activation, and it is characterized by an activation diameter, d_{act}. Unactivated particles are made of something, and here we assume that ammonium nitrate (acid and base) does not interact with the unactivated particles beyond the Kelvin effect. The activation diameter simply depends on supersaturation and so strictly scales with the square of the gas-phase concentrations (and thus activities) of the acid and base.

$$\begin{aligned} S_{AB,p} &= \frac{a_A^v a_B^v K_{AB}^{eq}}{K_{AB,p}^2} = 1 \\ 1 &= \frac{S_{AB}^\circ}{K_{AB,p}^2};\ S_{AB}^\circ = a_A^v a_B^v K_{AB}^{eq} \\ S_{AB}^\circ &= 10^{\left(2d_{K10,AB}/d_{act}\right)} \\ d_{act} &= \frac{2d_{K10,AB}}{\log_{10}\left(S_{AB}^\circ\right)} \end{aligned} \quad (13)$$

As stated above we treat the Kelvin diameter(s) as an adjustable parameter given the very small number of molecules in the activating clusters. However, we expect the values to lie somewhere between those of water ($d_{K10,H_2O} \simeq 1$ nm) and organics ($d_{K10,org} \simeq 6$ nm). If the growing particle is a quasi aqueous solution with $\sigma \simeq 75$ mN m^{-1}, we might

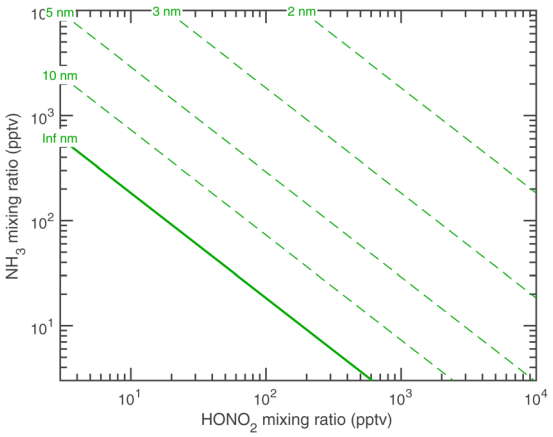

Fig. 12 Activation diameters at 263 K for solid ammonium nitrate with $d_{K10} = 3$ nm. Diameters are shown with contour labels, and $d_{act} = \infty$ at the saturation line $S = 1$. To the lower left of this saturation line particles will not activate. Unlike the growth rates, the activation diameters depend exponentially on the saturation ratios; for example, the 5 nm activation diagonal from upper right to lower left corresponds to $S \simeq 20$, whereas the smallest diameter shown (2 nm) corresponds to $S \simeq 1000$.

expect NH_3 to have $d_{K10,NH_3} \simeq 1$ nm and $HONO_2$ to have $d_{K10,HONO_2} \simeq 3.7$ nm, based solely on mass, with an average of about 2.4 nm.

Fig. 12 shows the activation diameters at 263 K for $d_{K10} = 3$ nm over this broad atmospheric range of $HONO_2$ and NH_3. The solid green activation threshold is identical to the saturation line ($S = 1$), with particles activating only in the supersaturated region to the upper right. The smallest activation diameters sit far from the saturation line because of the exponential dependence; this is in contrast to the regular spacing of the saturation contours in Fig. 10 and 11.

5.3 Overall flux balance solution

Eqn (8) shows that to find the growth rate we need to determine the uptake coefficient of the limiting species. We can combine the constraining expressions to write

$$\begin{aligned}
\gamma_{B,p} &= r^{v}_{AB}\gamma_{A,p} \\
\left[1 - \frac{a^{s}_{B,p}}{a^{v}_{B}}K_{B,p}\right] &= r^{v}_{AB}\left[1 - \frac{a^{s}_{A,p}}{a^{v}_{A}}K_{A,p}\right] \\
\left[1 - \frac{1}{S_{B,p}}\right] &= r^{v}_{AB}\left[1 - \frac{K_{A,p}}{a^{v}_{A}a^{s}_{B,p}K^{eq}_{AB}}\right] \\
&= r^{v}_{AB}\left[1 - \frac{K_{A,p}K_{B,p}a^{v}_{B}}{a^{v}_{A}a^{v}_{B}a^{s}_{B,p}K_{B,p}K^{eq}_{AB}}\right] \\
&= r^{v}_{AB}\left[1 - \frac{K^{2}_{AB,p}}{a^{v}_{A}a^{v}_{B}K^{eq}_{AB}}S_{B,p}\right] \\
&= r^{v}_{AB}\left[1 - \frac{S_{B,p}}{S_{AB,p}}\right] \\
S_{B,p} - 1 &= r^{v}_{AB}S_{B,p} - \frac{r^{v}_{AB}}{S_{AB,p}}(S_{B,p})^{2}
\end{aligned} \tag{14}$$

And so

$$\begin{aligned}
0 &= \frac{r^{v}_{AB}}{S_{AB,p}}(S_{B,p})^{2} + (1 - r^{v}_{AB})S_{B,p} - 1 \\
S_{B,p} &= \frac{r^{v}_{AB} - 1 \pm \sqrt{(r^{v}_{AB} - 1)^{2} + 4r^{v}_{AB}/S_{AB,p}}}{2r^{v}_{AB}/S_{AB,p}} \\
&= \frac{S_{AB,p}}{2}\left[\left(\frac{r^{v}_{AB} - 1}{r^{v}_{AB}}\right) + \sqrt{\left(\frac{r^{v}_{AB} - 1}{r^{v}_{AB}}\right)^{2} + \frac{4}{r^{v}_{AB}S_{AB,p}}}\right]
\end{aligned} \tag{15}$$

We take the positive root because we require a positive solution. This gives us the uptake coefficient for the limiting species (B here), from eqn (6). There are two natural variables here: the collision ratio, r^{v}_{AB}, and the saturation ratio, $S_{AB,p}$. These are more or less at 45° to the mixing ratio axes in the figures, with the origin at the intersection of the equi-collision diagonal (from the lower left to the upper right) and the saturation ($S = 1$) diagonal.

There are two important limits. The first is symmetrical condensation where the collision rates of NH_3 and $HONO_3$ are identical $r_{AB} = 1$. Here,

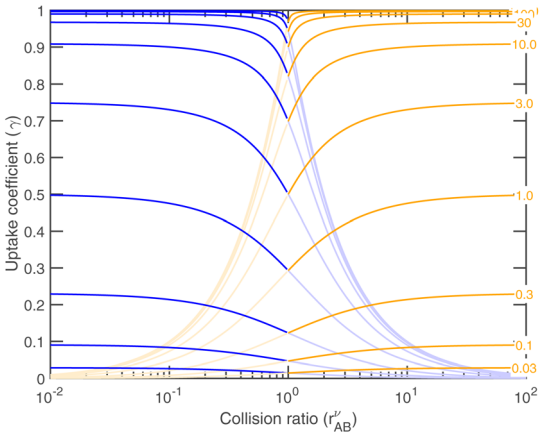

Fig. 13 Uptake coefficient *vs.* the collision ratio for different (excess) saturation ratios, $S - 1$, shown on the contours near the right-hand x axis. The uptake coefficient for the limiting vapor is shown as a darker curve, and for the excess vapor the curve is lighter. Acid ($HONO_2$) is shown in blue and is limiting (darker) for $r^{v}_{AB} < 1$. Base (NH_3) is shown in orange and is limiting (darker) for $r^{v}_{AB} \geq 1$. For $S = 10$ the uptake tends toward $\gamma \simeq 0.9$ and for $S = 1$ it tends toward $\gamma \simeq 0.5$ at the limit of a very high or very low collision ratio. A transition region lies within roughly a factor of 10 of equal vapor collision rates.

$$\lim_{r^{v}_{AB}\to 1} S_{B,p} = \sqrt{S_{AB,p}}$$

The second case is the opposite, with a large asymmetry ($r \to 0$ or $r \to \infty$).

$$\lim_{r^{v}_{AB}\to \infty} S_{B,p} = S_{AB,p}$$

As the collision ratio (asymmetry) increases the saturation ratio of the limiting species also increases from $\sqrt{S_{AB,p}}$ to $S_{AB,p}$. The limiting species will carry the full burden of sustaining the saturation ratio, as the excess species will be almost perfectly saturated; at this limit, the uptake coefficient, γ, will remain constant. This is shown in Fig. 13, which also shows γ drop away toward zero dramatically as the collision ratio switches from acid limited ($r^{v}_{AB} < 1$) to base limited ($r^{v}_{AB} > 1$), with the limiting species emphasized by darker (more saturated) curves over the range of excess saturation ratios, S^{xs}_{AB}. For large saturation ratios, $S^{xs}_{AB} \lesssim 10$, the uptake coefficient of the limiting species $\gamma \simeq 1$, with the exception of a small downward cusp at $r = 1$.

5.4 Growth rates

Returning to the growth rate in the "natural" coordinates of $S_{AB,p}$ and r^{v}_{AB}, with $r^{v}_{AB} > 1$ and growth thus limited by condensation of B, driven by a condensation rate of B toward the particles, $R^{gr}_{AB,p}$,

$$R^{gr}_{AB,p} = 2\frac{m_{AB,p}}{\rho_{AB,p}}s^{\perp}_{B,p}c^{v}_{B}\gamma_{B,p};\ \gamma_{B,p} = \frac{S^{xs}_{B,p}}{S_{B,p}} \tag{16}$$

This applies for either A or B at any r_{AB}, but for the limiting vapor as we have just seen, $\gamma \rightarrow 1$ (in many cases) whereas for the excess vapor $\gamma \rightarrow 0$ (in all cases). This is sufficient to determine the growth rate given measured concentrations of A and B (along with the thermodynamics). However, we would also like to contour growth rates for a given saturation ratio, $S_{AB,p}$, and for this we need c_B^v as a function of $S_{AB,p}$ and r_{AB}^v.

With the ideal gas vapor concentrations from eqn (1), the gas-particle equilibrium from eqn (12), and the collision ratio from eqn (10) we can derive the vapor concentration of the limiting reagent in terms of the natural coordinates.

$$c_B^v = \frac{s_{A,p}^{\perp}}{s_{B,p}^{\perp}} c_A^v \frac{1}{r_{AB}^v}$$

$$c_A^v = a_A^v \frac{p_A^\circ}{RT};\ c_B^v = a_B^v \frac{p_B^\circ}{RT}$$

$$a_A^v = \frac{K_{AB,p}^2}{a_B^v K_{AB}^{eq}} S_{AB,p}$$

This gives

$$\begin{aligned} c_A^v &= \frac{K_{AB,p}^2}{a_B^v K_{AB}^{eq}} \frac{p_A^\circ}{RT} S_{AB,p} \\ &= \frac{K_{AB,p}^2}{c_B^v K_{AB}^{eq}} \frac{p_A^\circ p_B^\circ}{(RT)^2} S_{AB,p} \\ c_B^v &= \frac{s_{A,p}^{\perp}}{s_{B,p}^{\perp}} \frac{K_{AB,p}^2}{c_B^v K_{AB}^{eq}} \frac{p_A^\circ p_B^\circ}{(RT)^2} \frac{S_{AB,p}}{r_{AB}^v} \\ c_B^v &= \sqrt{\frac{K_{AB,p}^2}{K_{AB}^{eq}} \frac{p_A^\circ p_B^\circ}{(RT)^2}} \sqrt{\frac{s_{A,p}^{\perp}}{s_{B,p}^{\perp}}} \sqrt{\frac{S_{AB,p}}{r_{AB}^v}} \end{aligned} \quad (17)$$

Fig. 14 shows the growth rates (in nm h^{-1}) at 263 K *versus* these natural coordinates for a range of excess saturation ratios. Combining with Fig. 13 we find, somewhat paradoxically, that, for any given saturation ratio, the limiting uptake coefficient, γ, reaches a (cusped) minimum at the equi-collision point, $r_{AB} = 1$, but the growth rate reaches a maximum at this same value. This is because both species are contributing to growth for $r_{AB} \simeq 1$. These natural coordinates of collision ratio and saturation ratio are roughly 45° from the concentration axes in Fig. 9–11. Because of this, for a constant total saturation ratio, the activity and thus concentration of the limiting gas-phase species will decrease as the collision ratio increases, and so the growth rate (as opposed to the uptake coefficient) will decrease, and for $r_{AB} \simeq 1$ the growth rate has a maximum even though the uptake coefficients have a minimum. Simply following the saturation ratio contours in Fig. 11 shows this clearly; the $r_{AB} = 1$ equi-collision spine is the diagonal running from lower left to upper right, and following a saturation ratio contour away from this spine shows steadily declining maximum growth rates. At very low excess saturation, the growth-rate curve in Fig. 14 is quite smooth, whereas at high excess saturation the curve takes on the sharp-peaked nature given by the sudden transition as the excess vapor changes identity at $r_{AB}^v = 1$ as shown in Fig. 11

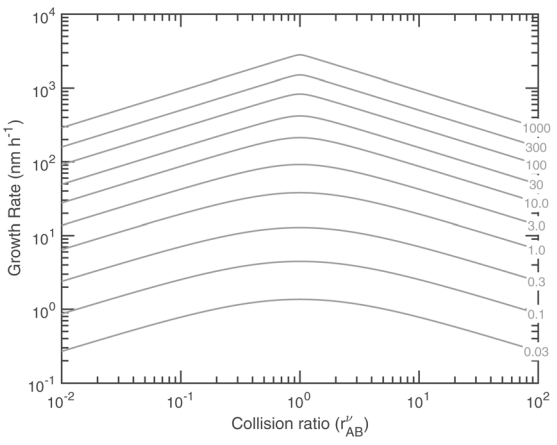

Fig. 14 Growth rate at 10 nm *vs.* the collision ratio for different excess saturation ratios (on contour labels) at 263 K (with no Kelvin term, *i.e.* $d_{K10} = 1$). At modest $S_{AB}^{xs} \lesssim 10$, the depression in γ for $r_{AB}^v \simeq 1$ rounds the growth rate curve in the center, whereas for greater saturation it remains sharp.

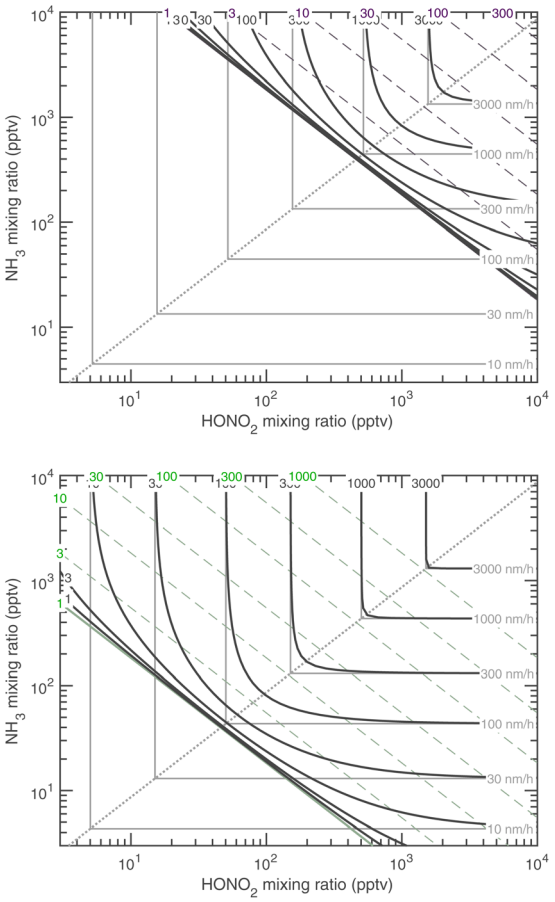

Fig. 15 Growth rate at 10 nm at 278 K (top, with dashed purple saturation ratio diagonal lines) and 263 K (bottom, with dashed green saturation ratio diagonal lines). These are the two temperatures shown for CLOUD data in Fig. 1. As with the "natural" growth coordinates, near the 1 : 1 equi-collision spine the growth rate is rounded compared to the sharp limiting values, with contours converging toward no growth at the $S = 1$ saturation diagonal line.

and the growth rate is always very near its maximum value. The smooth curve for $S \lesssim 3$ leads to the quadratic growth-rate dependence as shown in Fig. 1.

Fig. 15 combines these elements to show the growth rates of 10 nm particles in the ammonium nitrate phase space at 278 K and at 263 K. The black contours are at regular intervals of the growth rate (in nm h^{-1}) and, as expected, they bunch up near the $S_{AB} = 1$ saturation line. Above (to the upper right) that saturation line, with saturation ratios shown as dashed diagonals, the growth-rate contours ultimately approach the limiting maximum growth rates (in gray). For large S_{AB}, the contours even retain a sharp transition along the equi-collision spine, consistent with the near cusp in Fig. 14.

5.5 Temperature dependence

Almost all the temperature dependence in the system is caused by ammonium nitrate decomposition. Progressive cooling from 278 K to 223 K is shown in Fig. 15 (for warmer conditions) and Fig. 16 (for colder conditions). The colder axes in Fig. 16 are shifted by a factor of 100 toward low mixing ratios. The colored contours in each figure are the growth rate, and the color of the saturation ratio diagonals indicates the temperature (as in Fig. 1, purple is 278 K and green is 263 K). Starting at 223 K and warming, the progressive volatilization of the $HN_4 \cdot NO_3$ drives the saturation ($S = 1$) line, which sweeps from the lower left up along the equi-collision spine like a plow, gathering "isotachs" of constant growth rate as it moves toward the upper right.

Fig. 16 reflects free-tropospheric conditions whereas Fig. 15 reflects lower tropospheric and wintertime boundary layer conditions, where the actual mixing ratios of NH_3 and $HONO_2$ can be much higher. At 223 K the system is almost non-volatile, except that the constituents are still very volatile and so any excess will remain in the gas phase; however, growth by the limiting constituent is essentially kinetic. Conversely, by 278 K, any disequilibrium implies very rapid growth (or evaporation) – the saturation line is a stable attractor, and so in practice this means the system will equilibrate very rapidly. This is why air-

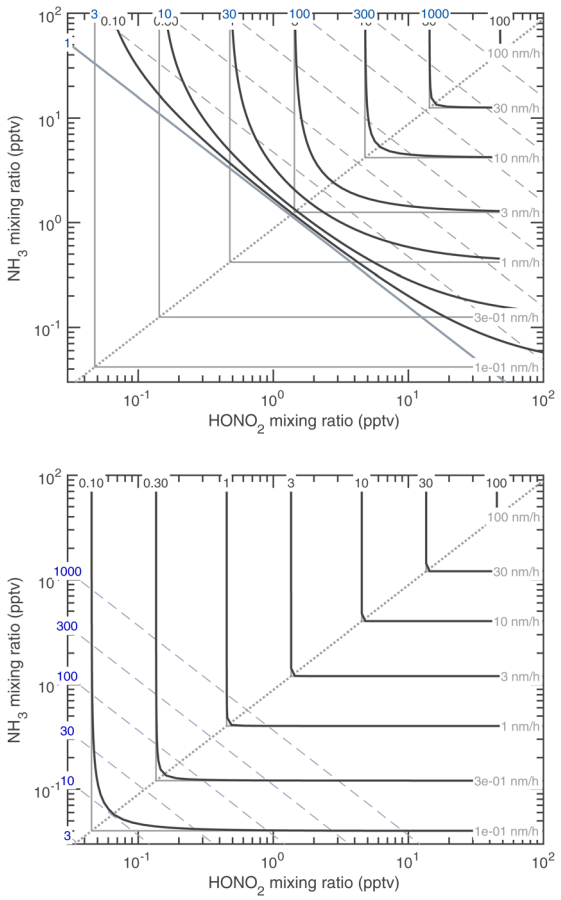

Fig. 16 Growth rate of 10 nm particles at 243 K (top) and 223 K (bottom). Note the axes shift by a factor of 100 compared to the warmer Fig. 15. At 223 K (*i.e.* in the upper troposphere), the only sign of reversible (semi-volatile) condensation by the limiting reagent is curvature near the equi-collision spine with both vapors below a 1 pptv mixing ratio and almost imperceptible growth of 0.1 nm h^{-1}.

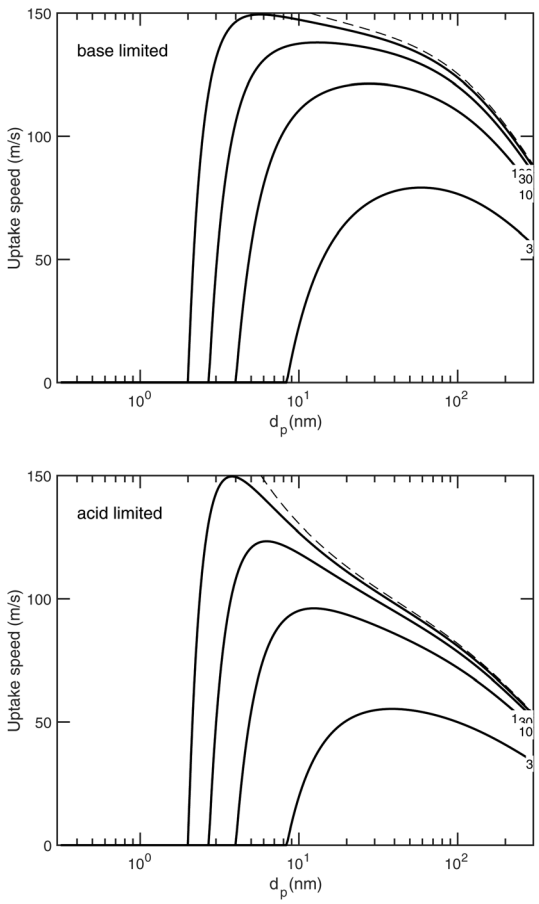

Fig. 17 Uptake speed ($\gamma_{i,p} s_{i,p}^{\perp}$, black curves) *vs.* the diameter for flat-surface saturation ratios $S° = \{3, 10, 30, 100\}$ and $d_{K10} = 2$ nm. The $S° = \infty$ limit is shown as a dashed curve. (Top) Base-limited (NH_3) limited uptake assuming no van der Waals enhancement ($A = 0$ joule). (Bottom) Acid-limited ($HONO_2$) uptake with significant van der Waals enhancement ($A = 6 \times 10^{-20}$ joule). The collision speed (and thus growth rates) increases rapidly after activation, reaches a maximum and then declines again. The maximum is especially sharp when the van der Waals enhancement is large (*i.e.* for acid limited conditions in the lower panel).

quality models often assume that ammonium nitrate is in equilibrium.[5]

5.6 Size dependent growth rates

We have been presenting growth rates as a semi-constant value (specified at a reference diameter, $d_p = 10$ nm but only considering the saturation ratio over a flat surface, S°_{AB}). However, we can define an uptake speed as the product of the collision speed and the uptake coefficient, $s^{up}_{i,p} = s^{\perp}_{i,p}\gamma_{i,p}$. The uptake speed (and thus the growth rate) is anything but a constant, as shown in Fig. 8. Some of those collisions do not result in uptake, even for the limiting vapor; as shown above this is especially pronounced for low saturation ratios. Once we know the uptake coefficient of the limiting species, γ_{lim}, we can consider the effective collision speed of that species as a function of size, which will be affected by the Kelvin term and thus incorporates the activation diameter (where the speed drops to zero). This is $s = \gamma s^{\perp}$, which we show in Fig. 17 for a collision asymmetry $r^{v}_{AB} = 10$ (so limited by ammonia) on top and $r^{v}_{AB} = 0.1$ (so limited by nitric acid) on bottom. For the purposes of illustration we assume negligible van der Waals enhancement for NH_3 and a large enhancement for $HONO_2$. For $S^\circ \gtrsim 10$, activation is quite rapid and the speed reaches its maximum value quite quickly, but for less saturated cases the size dependence has a broad maximum. This is especially dramatic for $HONO_2$-limited uptake, where the van der Waals term drops off sharply with a size difference between the colliding species (vapor and particle) and so the dipole – induced-dipole enhancement as mostly manifest below 10 nm. For cases near 1 : 1, the system will even switch between being acid limited for small size to being base limited for larger particles as the relative collision speeds of the two vapors change with particle size (as in Fig. 8).

6 CLOUD results

We can now compare our theoretical values for the activation diameter and growth rate to those observed at CLOUD. The CLOUD observations are shown in Fig. 1. We compare these to the theory in Fig. 18 and 19. Here we use a reference diameter $d_p = 30$ nm, more or less in the middle of the observed growth range for activated particles; however, especially for high growth rates, the absolute values are quite uncertain. The experiments were carried out with nucleation by ammonia and sulfuric acid. In some cases oxidized (aromatic) organic vapors may have contributed some growth but the experiments in this dataset had very low organic growth compared to the activated ammonium nitrate growth.[6] However, the composition and interactions below or near the activation diameter are not known precisely. For this reason, we treat the Kelvin diameter as an unknown parameter.

Fig. 18 shows that the activation at 278 K is consistent with theory for a small $d_{K10} = 1$ nm. This is similar to water and somewhat smaller than the expected 2.5 nm or so; the experiment did include oxidized aromatic organic compounds as well, and it is possible that some co-condensing HOMs were surface

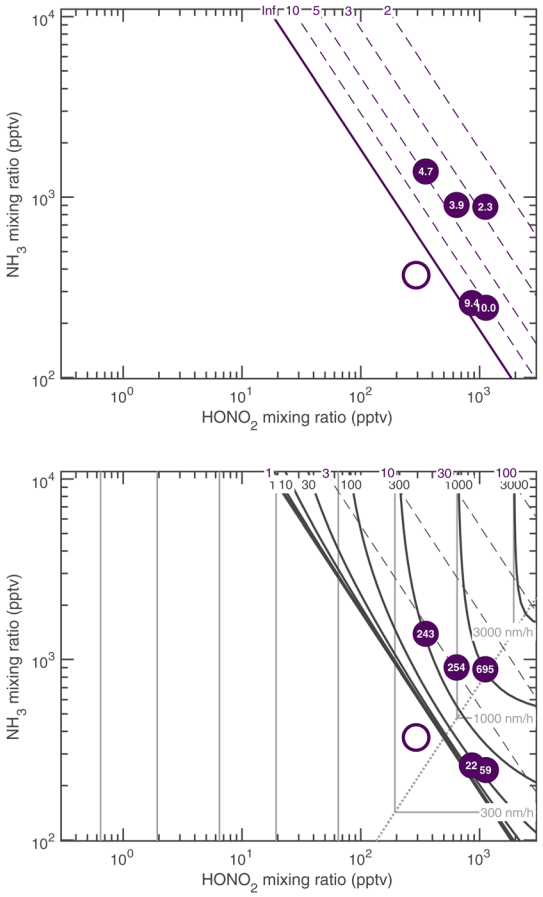

Fig. 18 Activation diameter (top) and activated growth rate at d_p = 30 nm (bottom) for 278 K comparing theory and CLOUD observations, with $d_{K10} = 1$ nm. Observed values are indicated with a number within each symbol. One case, with the open circle, did not activate and sits below (to the lower left) of the saturation line. The activation diameters show the expected exponential dependence with an increasing saturation ratio, and the growth rates increase sharply away from the saturation line as well.

active and able to drop the surface tension from a water-like 75 mN m^{-1} to a more organic-like 30 mN m^{-1}, which would quantitatively explain the observations. The predicted and observed growth rates in Fig. 18 are consistent, including the experiment in undersaturated conditions. These data are all near the equi-collision spine and most of the variation in both the activation diameter and growth rate appears to be due to variation in NH_3.

Fig. 19 shows that the activation at 263 K is reasonably consistent with theory for $d_{K10} = 2.5$ nm. This suggests a more aqueous-like activating particle, perhaps with less surfactant. However, these activating particles contain between 10 and 100 $NH_4 \cdot NO_3$, and so bulk behavior is far from assured. The growth rates are now well into the $HONO_2$-limited regime, and while they qualitatively agree well with theory, observed growth above 100 nm h^{-1} is significantly faster than predicted (by about a factor of 5). Overall the agreement is good, though the fastest growth rates are not perfectly reproduced, and the Kelvin diameter remains a free (ish) parameter.

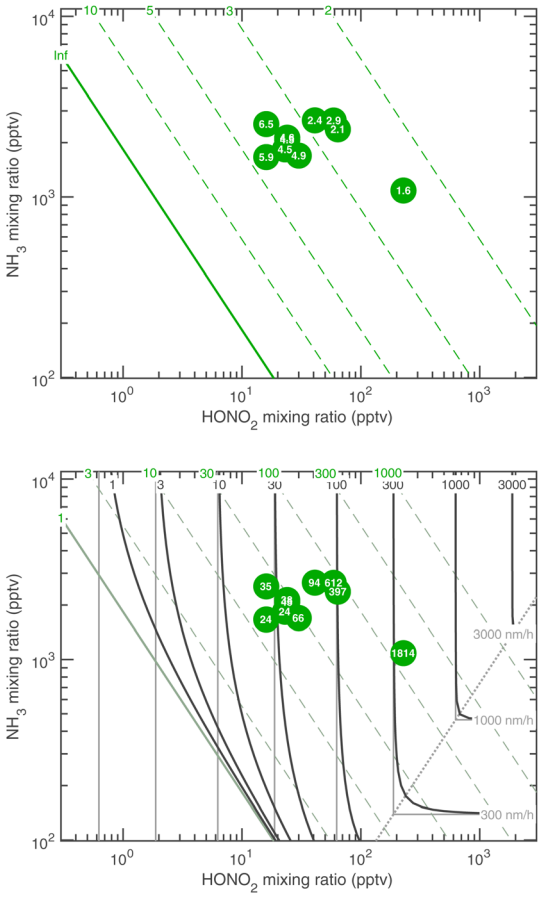

Fig. 19 Activation diameter (top) and activated growth rate at d_p = 30 nm (bottom) for 263 K comparing theory and CLOUD observations, with d_{K10} = 2.5 nm. Observed values are indicated with a number within each symbol. Wintertime megacity conditions with 2–20 pptv $HONO_2$ and 2 ppb NH_3 will sustain growth at 3–30 nm h^{-1} well below 10 nm.

7 Atmospheric significance

Any unified aerosol system (such as the atmosphere) will move toward the equilibrium $S_{AB} = 1$ line without a cause sustaining any supersaturation. If it is supersaturated, condensation will deplete the excess vapor (after driving particle growth), and if it is undersaturated, evaporation will be a source of vapors. The timescale for reaching a steady state will be the collision frequency of vapors with the particles (the condensation sink).[18] If there is a source of vapors (*i.e.* photochemical production of $HONO_2$ or uniform emission of NH_3), the system will relax toward a steady state with that production balancing the condensational loss. However, transient events may also be important, because rapid growth for only a few minutes can carry nucleated particles through the "valley of death" between 2 and 10 nm where coagulation loss is high and survival probability is low. These transients can be driven by chemical production, transport, or steady temperature change.

A box model based on the microphysics presented here and simulating the CLOUD conditions for these experiments reproduces the observed behavior in CLOUD. Simulations show that the survival probability of nucleated particles is greatly increased with the rapid growth driven by ammonium nitrate condensation.[7] Further simulations show that transient increases in the saturation ratio simulating turbulent vertical transport in the boundary layer can drive brief pulses of growth from the smallest sizes, thus enhancing the average survival probability.[9] In the real world, ambient observations of size distributions evolving over hours at a fixed surface site within spatially inhomogeneous conditions may well render these pulses difficult to discern. However, the nearly irreversible condensational growth described here will occur whenever it is cold enough for substantial saturation ratios to be sustained, either *via* temperature changes (specifically uplift) or chemical production (of nitric acid vapor). We thus expect it to be important for particle growth well below 10 nm in both the wintertime boundary layer[6] (even for modest 3–10 nm h^{-1} growth rates limited by $HONO_2$ production) and throughout the upper troposphere.[8,19] To address this, chemical transport models will need to either treat the condensation dynamics directly or implement a hybrid solution to condense ammonium nitrate in proportion to the aerosol volume under equilibrium conditions and in proportion to the aerosol surface area under dynamic steady state conditions.[20]

8 Conclusions

The theory of semi-volatile reactive uptake is straightforward for a simple system with well constrained thermodynamics, such as ammonium nitrate. Considering the dual constraints of dynamics (condensation speeds) and thermodynamics (saturation ratios), and especially how saturation ratios change with temperature, we are able to develop a framework for visualizing the transition from semi-volatile equilibration to irreversible uptake that predicts both activation diameters and growth rates. This framework reproduces observations from the CERN CLOUD experiment.

Data availability

All data used in this work are in the literature, and all parameters are in the text.

Author contributions

NMD conceived the project and designed the overall scope. MX inspired the framework and wrote an initial version of the dynamical model. NMD wrote the manuscript along with DS and IEH, with editorial input from all coauthors.

Conflicts of interest

The authors declare no conflicts.

Acknowledgements

This work was supported by Grant AGS2132089 from the U.S. National Science Foundation; the Vienna Science and

Technology Fund (WWF) through project VRG22-003; grant 200021_213071 and PZ00P2_216181 from the Swiss National Science Fund.

Notes and references

1 M. Mozurkewich, *Atmos. Environ., Part A*, 1993, **27**, 261–270.
2 J. A. Duisman and S. A. Stern, *J. Chem. Eng. Data*, 1969, **14**, 457–459.
3 L. Haar and J. S. Gallagher, *J. Phys. Chem. Ref. Data*, 1978, **7**, 635–792.
4 C. Fountoukis and A. Nenes, *Atmos. Chem. Phys.*, 2007, **7**, 4639–4659.
5 E. R. Trump, C. Fountoukis, N. M. Donahue and S. N. Pandis, *Atmos. Environ.*, 2015, **102**, 274–281.
6 M. Wang, W. Kong, R. Marten, X.-C. He, D. Chen, J. Pfeifer, A. Heitto, J. Kontkanen, L. Dada, A. Kurten, T. Yli-Juuti, H. E. Manninen, S. Amanatidis, A. Amorim, R. Baalbaki, A. Baccarini, D. M. Bell, B. Bertozzi, S. Brakling, S. Brilke, L. C. Murillo, R. Chiu, B. Chu, L.-P. D. Menezes, H. Finkenzeller, L. G. Carracedo, M. Granzin, R. Guida, A. Hansel, V. Hofbauer, J. Shen, J. Duplissy, K. Lehtipalo, H. Lamkaddam, M. Lampimaki, C. P. Lee, V. Makhmutov, G. Marie, S. Mathot, R. L. Mauldin III, B. Mentler, T. Muller, A. Onnela, E. Partoll, T. Petaja, M. Philippov, V. Pospisilova, A. Ranjithkumar, M. Rissanen, B. Rorup, W. Scholz, M. Simon, M. Sipila, G. Steiner, D. Stolzenburg, Y. J. Tham, A. Tome, A. C. Wagner, D. S. Wang, S. K. Weber, P. M. Winkler, P. J. Wlasits, Y. Wu, M. Xiao, Q. Ye, M. Zauner-Wieczorek, X. Zhou, R. Volkamer, I. Riipinen, J. Dommen, J. Curtius, U. Baltensperger, M. Kulmala, D. R. Worsnop, J. Kirkby, J. H. Seinfeld, I. El-Haddad, R. C. Flagan and N. M. Donahue, *Nature*, 2020, **581**, 184–189.
7 R. Marten, M. Xiao, B. Rörup, M. Wang, W. Kong, X.-C. He, D. Stolzenburg, J. Pfeifer, G. Marie, D. S. Wang, W. Scholz, A. Baccarini, C. P. Lee, A. Amorim, R. Baalbaki, D. M. Bell, B. Bertozzi, L. Caudillo, B. Chu, L. Dada, J. Duplissy, H. Finkenzeller, L. G. Carracedo, M. Granzin, A. Hansel, M. Heinritzi, V. Hofbauer, D. Kemppainen, A. Kürten, M. Lampimäki, K. Lehtipalo, V. Makhmutov, H. E. Manninen, B. Mentler, T. Petäjä, M. Philippov, J. Shen, M. Simon, Y. Stozhkov, A. Tomé, A. C. Wagner, Y. Wang, S. K. Weber, Y. Wu, M. Zauner-Wieczorek, J. Curtius, M. Kulmala, O. Möhler, R. Volkamer, P. M. Winkler, D. R. Worsnop, J. Dommen, R. C. Flagan, J. Kirkby, N. M. Donahue, H. Lamkaddam, U. Baltensperger and I. El Haddad, *Environ. Sci.: Atmos.*, 2022, **2**, 491–499.
8 M. Wang, M. Xiao, B. Bertozzi, G. Marie, B. Rörup, B. Schulze, R. Bardakov, X.-C. He, J. Shen, W. Scholz, R. Marten, L. Dada, R. Baalbaki, B. Lopez, H. Lamkaddam, H. E. Manninen, A. Amorim, F. Ataei, P. Bogert, Z. Brasseur, L. Caudillo, L.-P. D. Menezes, J. Duplissy, A. M. L. Ekman, H. Finkenzeller, L. G. Carracedo, M. Granzin, R. Guida, M. Heinritzi, V. Hofbauer, K. Höhler, J. E. Krechmer, A. Kürten, K. Lehtipalo, N. G. A. Mahfouz, V. Makhmutov, D. Massabò, S. Mathot, R. L. Mauldin, B. Mentler, T. Müller, A. Onnela, T. Petäjä, M. Philippov, A. A. Piedehierro, A. Pozzer, A. Ranjithkumar, M. Schervish, M. Simon, Y. Stozhkov, A. Tomé, N. S. Umo, F. Vogel, R. Wagner, D. S. Wang, S. K. Weber, A. Welti, Y. Wu, M. Zauner-Wieczorek, M. Sipilä, P. M. Winkler, A. Hansel, U. Baltensperger, M. Kulmala, R. C. Flagan, J. Curtius, I. Riipinen, H. Gordon, J. Lelieveld, I. El-Haddad, R. Volkamer, D. R. Worsnop, T. Christoudias, J. Kirkby, O. Möhler and N. M. Don, *Nature*, 2022, **605**, 483–489.
9 R. Marten, M. Xiao, M. Wang, W. Kong, X.-C. He, D. Stolzenburg, J. Pfeifer, G. Marie, D. S. Wang, A. Baccarini, C. P. Lee, A. Amorim, R. Baalbaki, D. M. Bell, B. Bertozzi, L. Caudillo, L. Dada, J. Duplissy, H. Finkenzeller, M. Heinritzi, M. Lampimäki, K. Lehtipalo, H. E. Manninen, B. Mentler, A. Onnela, T. Petäjä, M. Philippov, B. Rörup, W. Scholz, J. Shen, Y. J. Tham, A. Tomé, A. C. Wagner, S. K. Weber, M. Zauner-Wieczorek, J. Curtius, M. Kulmala, R. Volkamer, D. R. Worsnop, J. Dommen, R. C. Flagan, J. Kirkby, N. M. Donahue, H. Lamkaddam, U. Baltensperger and I. E. Haddad, *Environ. Sci.: Atmos.*, 2024, **4**, 265–274.
10 N. M. Donahue, W. K. Chuang and M. SchervishGas-Phase Organic Oxidation Chemistry and Atmospheric Particles, in *Advances in Chemistry of the Contemporary Atmosphere*, ed. J. R. Barker, A. Steiner and T. J. Wallington, World Scientific, 2019, vol. 2, ch, pp. 199–317.
11 C. Larriba, C. J. Hogan Jr, M. Attoui, R. Borrajo, J. F. Garcia and J. F. de la Mora, *Aerosol Sci. Technol.*, 2011, **45**, 453–467.
12 H. C. Hamaker, *Physica*, 1937, **4**, 1058–1072.
13 J. E. Brockmann, P. H. M. Murry and B. Y. H. Liu, *J. Colloid Interface Sci.*, 1982, **88**, 522–529.
14 J. Julin, P. M. Winkler, N. M. Donahue, P. E. Wagner and I. Riipinen, *Environ. Sci. Technol.*, 2014, **48**, 12083–12089.
15 D. Stolzenburg, M. Simon, A. Ranjithkumar, A. Kürten, K. Lehtipalo, H. Gordon, T. Nieminen, L. Pichelstorfer, X. He, S. Brilke, M. Xiao, A. Amorim, R. Baalbaki, A. Baccarini, L. Beck, S. Bräkling, L. C. Murillo, D. Chen, B. Chu, L. Dada, A. Dias, J. Dommen, J. Duplissy, I. E. Haddad, H. Finkenzeller, L. Fischer, L. G. Carracedo, M. Heinritzi, C. Kim, T. K. Koenig, W. Kong, H. Lamkaddam, C. P. Lee, M. Leiminger, Z. Li, V. Makhmutov, H. E. Manninen, G. Marie, R. Marten, T. Müller, W. Nie, E. Partol, T. Petäjä, J. Pfeifer, M. Philipov, M. P. Rissanen, B. Rörup, S. Schobesberger, S. Schuchmann, J. Shen, M. Sipilä, G. Steiner, Y. Stozhkov, C. Tauber, Y. J. Tham, A. Tomé, M. Vazquez-Pufleau, A. C. Wagner, M. Wang, Y. Wang, S. K. Weber, D. Wimmer, P. J. Wlasits, Y. Wu, Q. Ye, M. Zauner-Wieczorek, U. Baltensperger, K. S. Carslaw, J. Curtius, N. M. Donahue, R. C. Flagan, A. Hansel, M. Kulmala, R. Volkamer, J. Kirkby and P. M. Winkler, *Atmos. Chem. Phys.*, 2020, **20**, 7359–7372.
16 I. Riipinen, T. Yli-Juuti, J. R. Pierce, T. Petäjä, D. R. Worsnop, M. Kulmala and N. M. Donahue, *Nat. Geosci.*, 2012, **5**, 453–458.

17 M. Kulmala, V.-M. Kerminen, T. Petäjä, A. J. Ding and L. Wang, *Faraday Discuss.*, 2017, **200**, 271–288.
18 R. Saleh, N. M. Donahue and A. L. Robinson, *Environ. Sci. Technol.*, 2013, **47**, 5588–5594.
19 C. J. Williamson, A. Kupc, D. Axisa, K. R. Bilsback, T. Bui, P. Campuzano-Jost, M. Dollner, K. D. Froyd, A. L. Hodshire, J. L. Jimenez, J. K. Kodros, G. Luo, D. M. Murphy, B. A. Nault, E. A. Ray, B. Weinzierl, J. C. Wilson, F. Yu, P. Yu, J. R. Pierce and C. A. Brock, *Nature*, 2019, **574**, 399–403.
20 J. R. Pierce, I. Riipinen, M. Kulmala, M. Ehn, T. Petäjä, H. Junninen, D. R. Worsnop and N. M. Donahue, *Atmos. Chem. Phys.*, 2011, **11**, 9019–9036.